Journal of Colloid and Interface Science 534 (2019) 357–369

Contents lists available at ScienceDirect

Journal of Colloid and Interface Science

journal homepage: www.elsevier.com/locate/jcis

In-situ deposition of gold nanoparticles onto polydopamine-decorated g-C_3N_4 for highly efficient reduction of nitroaromatics in environmental water purification

Lei Qin [1], Danlian Huang [1], Piao Xu [1], Guangming Zeng *, Cui Lai *, Yukui Fu, Huan Yi, Bisheng Li, Chen Zhang, Min Cheng, Chengyun Zhou, Xiaofeng Wen

College of Environmental Science and Engineering, Hunan University, Changsha 410082, PR China
Key Laboratory of Environmental Biology and Pollution Control, Hunan University, Ministry of Education, PR China

GRAPHICAL ABSTRACT

Efficient reduction of nitroaromatics by PDA-g-C_3N_4/Au catalyst.

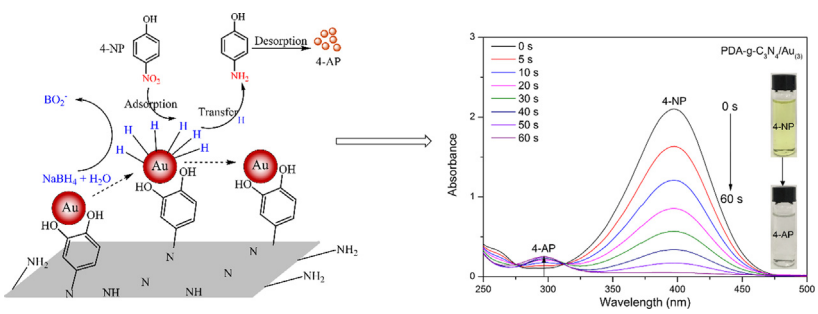

ARTICLE INFO

Article history:
Received 31 July 2018
Revised 12 September 2018
Accepted 15 September 2018
Available online 17 September 2018

Keywords:
Au catalysts
Polydopamine
g-C_3N_4
Nitroaromatics
Reduction

ABSTRACT

A green synthesized gold-catalyst (PDA-g-C_3N_4/Au) for highly efficient reduction of nitroaromatics by $NaBH_4$ was proposed. Polydopamine (PDA) served as the reductant and stabilizer for AuNPs reduction, avoiding the use of chemical reductant and stabilizer that may result in secondary contamination. g-C_3N_4 not only acted as the support but also provided compatibility for AuNPs deposition, enhancing the stability and deposition of AuNPs, which improved the catalytic activity. Different experimental parameters including the amount of Au loading, concentration of $NaBH_4$, and dosage of catalyst were studied. Results showed that PDA-g-C_3N_4/$Au_{(3)}$ revealed higher catalytic activity with a rate constant of 0.0514 s^{-1} and TOF of 545.60 h^{-1} for 4-NP reduction. In addition, the catalyst was highly efficient in reduction of other nitroaromatics and the reduction rates of these compounds were found as the sequence: methyl orange > 2-nitrophenol > 2, 4-dinitrophenol > Erichrome Black T > Congo red. Moreover, the PDA-g-C_3N_4/$Au_{(3)}$ catalyst kept high stability and excellent conversion efficiency over ten reduction cycles. The practical application on different real water samples suggests that this Au catalyst has promising application in environmental water purification. The simple and green synthetic Au catalyst expands the range of application and provides potential application on environmental remediation.

* Corresponding authors at: College of Environmental Science and Engineering, Hunan University, Changsha, Hunan 410082, PR China.
E-mail addresses: zgming@hnu.edu.cn (G. Zeng), laicui@hnu.edu.cn (C. Lai).

[1] These authors contribute equally to this article.

https://doi.org/10.1016/j.jcis.2018.09.051
0021-9797/© 2018 Published by Elsevier Inc.

1. Introduction

In recent years, the noble nanoparticles like gold (Au), silver (Ag), palladium (Pd), and platinum (Pt) have gained tremendous application in the generation of chemicals and fuels [1,2]. They are important for environmental protection because of the unique optical and electronic properties, as well as the potential application as an alternative class of efficient catalysts [3–5]. Among them, gold nanoparticles (AuNPs) have been demonstrated as one of high-efficiency catalysts in a great number of redox reactions even at low temperature, because they are proven to have large surface-to-volume ratio and more negative Fermi potential [6,7]. As for the reactions catalyzed by AuNPs, the reduction of nitroaromatics is of great significance in the fields of environment and chemical industry due to the pollutant nature of these compounds and the practical value of the reduction products [8–11]. For example, 4-aminophenol (4-AP), the reduction product of 4-nitropheol (4-NP), is found applications as drying agent, corrosion inhibitor, and precursor for the fabrication of some drugs [12,13]. In addition, compared with other noble nanoparticles, AuNPs have the unique properties of strongly size-dependent property. Smaller size, higher catalytic activity shows at mild conditions, even at low temperature [14]. However, free AuNPs are easy to aggregation because of the high surface energy, thus leading to a certain decay of catalytic activity, poor durability, and low recyclability [15]. In this case, researchers tend to immobilize AuNPs on the supports dispersedly.

Graphitic carbon nitride (g-C_3N_4), an easy-gained sustainable and environmentally friendly material, has attracted growing interest as graphene-like structure that reveals good electrical, thermal, and mechanical properties [16–21]. Abundant amine groups on the surface of g-C_3N_4 provide compatibility for anchoring metal nanoparticles [22]. The presence of nitrogen groups on the surface of carbon support can reduce the size and enhance the stability of nanoparticles [23–27]. These characteristics allow g-C_3N_4 an ideal support for anchoring AuNPs as gold-based catalyst. For example, Wang et al. [28] have prepared an Au/g-C_3N_4 hybrid for bacteria killing and wound disinfection by catalyzing the decomposition of H_2O_2 to $^{\bullet}OH$ radicals, in which g-C_3N_4 possess intrinsic peroxidase-like activity and plays the role on a synergetic nanozyme with AuNPs. With the excellent electron transfer ability of g-C_3N_4, Fu et al. [29] have used the Au/g-C_3N_4 contact system for reduction of 4-nitrophenol (4-NP) in the dark and under visible light irradiation. The synergistic effect of Au and g-C_3N_4 makes charge-transfer effect, which contributes to negative shift in Fermi level of Au. Besides, the N-contaning structure renders g-C_3N_4 possess strong proton (H^+) adsorption ability, which may be beneficial to H^+ transfer of nitroaromatics reduction [30–32]. Nevertheless, the deposition of AuNPs on g-C_3N_4 always needs precipitant or reducing agent whether using the deposition precipitation method or traditional AuNPs reducing method (e.g. Turkevich–Frens method or Brust–Schiffrin strategy) [33–35]. Most of these chemical reagents raise environmental concerns, which limits the biocompatibility and biomedical application [36]. Therefore, a reliable and bio/eco-friendly "green" chemical process for deposition AuNPs on g-C_3N_4 support is of great importance.

Dopamine (DA), a neurotransmitter, widely exists in the animal brain. It has drawn great attention since it contains plenty of amine and catechol functional groups and has the ability to adhere to the surface of many materials [37,38]. Especially, it can be self-polymerized to form polydopamine (PDA) under mild conditions (weakly alkaline pH) [39,40]. This process is simple, green, and low-cost. Moreover, numerous catechol groups of PDA are believed an alternative for synthesis of AuNPs due to the obvious reductive and stabilizing ability [38,41–43]. In view of this, PDA decorated g-C_3N_4 for Au catalyst synthesis shows the potential to improve the inherent property of Au catalyst and provide high catalytic activity. In this work, a PDA-g-C_3N_4 supported Au catalyst was prepared for highly efficient reduction of various nitroaromatics. The AuNPs were obtained via in-situ reduction of chloroauric acid by PDA. The effects of some experimental parameters on the catalytic performance were discussed in detail. To investigate the catalytic performance of described Au catalyst, some typical nitroaromatics like 2-nitrophenol (2-NP), 4-NP, 2, 4-dinitrophenol (2, 4-DNP), methyl orange (MO), Congo red (CR), and Erichrome Black T (EBT) were used as the targets. Additionally, reduction of 4-NP was used as the model reaction throughout the experiment and the catalytic performance on real water samples was proposed as well.

2. Experimental

2.1. Chemicals

Chloroauric acid hydrated ($HAuCl_4{\cdot}4H_2O$), melamine, sodium borohydride ($NaBH_4$), 2-amino-2-hydroxymethylpropane-1,3-diol (Tris), hydrochloric acid (HCl), and 4-Nitrophenol were purchased from the Sinopharm Chemical Reagent Co., Ltd (Shanghai, China). The ultrapure water (18.2 Ω, Milli-Q Millipore) was used in whole experimental process. Dopamine hydrochloride was gained from the Aladdin Bio-Chemical Technology Co., ltd (Shanghai, China). 2-nitrophenol, 4-nitrophenol, 2, 4-dinitrophenol, methyl orange, Congo red, and Erichrome Black T were obtained from Sinopharm Chemical Reagent Co., Ltd (Shanghai, China). All of the chemicals were used as obtained without further purification.

2.2. Characterization

The UV–Vis spectra were measured by a UV-2007 spectrometer (Shimadzu corporation, Kyoto, Japan) to obtain the absorption spectra with a quartz cuvette (1-cm pathlength). Transmission electron microscopy (TEM) and high-resolution transmission electron microscopy (HRTEM) images were measured on a TECNAI G2 F20 high-resolution transmission electron microscope with an accelerating voltage of 200 kV (FEI Company, Hillsboro, USA). The morphologies were recorded by scanning transmission electron microscopy (SEM, JSM-5600, Japan). The crystal structure of samples was realized in an X-ray diffraction analyzer with scan rate of 6° min^{-1} (XRD, radiation Bruker Smart-Apex-II, Cu Kα, λ = 0.1541 nm, Bruker, Germany). The elements and chemical state analyses were carried out by the X-ray photoelectron spectra (XPS) performed on a multifunctional imaging electron spectrometer using Al Kα radiation (Thermo ESCALAB 250XI, Thermo Scientific, USA). The Chemical transformation on the samples surface was performed on Fourier transform-infrared spectra (FT-IR, NICOLET 5700, Thermo Nicolet, USA). The contents of Au in different catalysts were measured by the inductively coupled plasma optical emission spectrometer (ICP-OES, Agilent 725 ICP-OES, USA).

2.3. Preparation of PDA-g-C_3N_4/Au catalyst

2.3.1. Preparation of g-C_3N_4

The bulk g-C_3N_4 was obtained by direct polymerization under high temperature. Typically, 10 g of melamine was carefully placed in an alumina crucible with cover and then kept into the center of the muffle furnace. The alumina crucible was first heated at 600 °C with a heating rate of 5 °C min^{-1} and maintained at 600 °C for 2 h and finally cooled down to room temperature naturally. The fabricated bulk g-C_3N_4 was further triturated for use.

2.3.2. Preparation of PDA-g-C_3N_4/Au catalyst

The PDA-g-C_3N_4 carrier was synthesized by a self-polymerizing process of DA molecules under weakly alkaline pH [44]. All the glassware was cleaned by freshly prepared chromic acid lotion before use. Briefly, 0.6 g of dopamine hydrochloride was firstly dissolved in 300 mL of Tris-HCl buffer (10 mM pH 8.5). Later, 0.6 g of prepared bulk g-C_3N_4 was dispersed in 300 mL of aforementioned DA-Tris solution, and then was treated under ultrasound for 30 min to disperse adequately. After ultrasonic treatment, the DA-Tris solution was allowed to stir continuously for 24 h at room temperature, accompanied by a turbid yellow-to-faint gray color change. After stirring, the mixture was washed using ultrapure water with 3 times and followed by drying in a vacuum oven.

In a typical preparation of PDA-g-C_3N_4/Au catalyst, 300 mg of PDA-g-C_3N_4 carrier was suspended in 250 mL of $HAuCl_4$ aqueous solution. The mixture was further stirred for 24 h under room temperature. The resultant catalyst was separated by filtering and washing with ultrapure water for at least 3 times. Finally, the as-prepared catalyst was dried in a vacuum oven for 24 h. In order to investigate the influence of Au loadings on catalytic activity, different amounts of $HAuCl_4$ (1, 2, 3, 4 mL of 1% $HAuCl_4{\cdot}4H_2O$ solution) were added to form different amount of Au loadings-based PDA-g-C_3N_4/Au catalyst, which were denoted as PDA-g-C_3N_4/$Au_{(1)}$, PDA-g-C_3N_4/$Au_{(2)}$, PDA-g-C_3N_4/$Au_{(3)}$, and PDA-g-C_3N_4/$Au_{(4)}$, respectively.

2.4. Catalytic reduction performance of nitroaromatics

To explore the catalytic activity and reusability of prepared PDA-g-C_3N_4/Au catalyst, reduction of nitroaromatics with $NaBH_4$ was carried out at ambient temperature. Briefly, 0.2 mM of 2-NP, 4-NP, 2, 4-DNP, MO, CR, and EBT were prepared respectively and different concentrations of $NaBH_4$ (10, 20, 40, 60, 80 mM) were freshly prepared. First, 15 mL prepared 4-NP and 15 mL $NaBH_4$ were mixed for minutes. Then, 5 mg aforementioned Au catalyst was added in the mixture. The color of the solutions gradually vanished with time. The reaction progress was detected by UV–Vis spectrometry at a certain time interval. After the reaction process completed, the catalyst was separated by centrifugal filtration and washed with ethyl alcohol and water for several times. Finally, the catalyst was dried in a vacuum oven for the next cycle. The reusability for the catalyst was proposed as the above process. The reduction of other nitroaromatics were determined as the same condition of 4-NP. Additionally, in order to investigate the catalytic performance on real water, different water samples including bottled water, tap water, lake water, and river water were collected from convenience store, our laboratory, Lake of Peach, and Hsiang River (Changsha, China), respectively. These samples were filtered through a 0.22 μm syringe filter to remove impurities first. The UV–Vis spectra of them were measured to confirm whether there was 4-NP in these samples. Subsequently, these samples were spiked with the standard solution of 4-NP and the final concentration of 4-NP was 0.2 mM. Finally, the catalytic process of these samples was proposed as the same with the reduction of 4-NP in ultrapure water. All of these results were obtained by three parallel experiments and were given as the average of these measurements by their standard deviations.

3. Results and discussion

3.1. Characterization of PDA-g-C_3N_4/Au catalyst

The morphology and size of prepared nanoparticles are shown in the TEM and HRTEM images (Fig. 1). As shown in Fig. 1a, the PDA-g-C_3N_4 support is successfully prepared, the sheet-like g-C_3N_4 and amorphous PDA layer are observed clearly, which are consistent with the SEM images (Fig. S1). In Fig. 1b, AuNPs are well deposited on the surface of PDA-g-C_3N_4. HRTEM image of PDA-g-C_3N_4/$Au_{(3)}$ (the insert of Fig. 1b) suggests the characteristic lattice fringes with the crystal plane distances of 0.204 and 0.235 nm, which are indexed to the spacing of the (2 2 0) and (1 1 1) planes of AuNPs respectively. Fig. 1c shows the scanning TEM (STEM) of as-prepared PDA-g-C_3N_4/$Au_{(3)}$, and the corresponding Au particle size distribution is shown in Fig. 1d with the average diameter of 26.1 ± 4.7 nm. In addition, the surface morphology of prepared bulk g-C_3N_4, PDA-g-C_3N_4 support, and PDA-g-C_3N_4/$Au_{(3)}$ catalyst were investigated by SEM (Fig. S1). It is obvious that many AuNPs are dispersedly deposited on the supports and most of them are spherical, while a few are polygonal and rodlike (Fig. S1c). The different shapes of AuNPs indicate different growth and aggregation processes of AuNPs are present. The irregular shapes of Au nanocrystals are often owing to the different nucleation species, faster particle growth and aggregation processes. This is analogous with the biological synthesis methods [45,46]. Corresponding energy dispersive spectrometer measurement reveals the successful preparation of g-C_3N_4. The atomic percent of C and N is almost 3:4, which is in good accordance with the structure of g-C_3N_4 (Fig. S1a). For the PDA-g-C_3N_4 support, the presence of O element is mainly due to the introduction of DA (Fig. S1b).

The XRD of g-C_3N_4, PDA-g-C_3N_4, and different amount of Au loadings-based PDA-g-C_3N_4/Au catalysts are presented in Fig. 2. As shown in Fig. 2, there are two diffraction peaks at 13.02° and 27.5° of g-C_3N_4, which can be indexed to the (1 0 0) and (0 0 2) diffraction planes of graphitic materials (JCPDS 87-1526), respectively. The weaker peak at 13.02° is due to the in-plane structural periods of tri-s-triazine units with the distance of 0.68 nm, which is the similar with the reported papers [29,47]. The strong peak at 27.5° is assigned to a typical stacking interlayer diffraction of graphitic-like structures corresponding to an interlayer distance of 0.324 nm, which is smaller than that of graphite (d = 0.336 nm) [48]. After self-polymerized by PDA, the XRD pattern of PDA-g-C_3N_4 is similar with pure g-C_3N_4, which indicates that the presence of PDA does not change the crystalline phase of g-C_3N_4. Nevertheless, the coating of PDA still affects the interlayer distances of g-C_3N_4. After different amount of Au loaded, the peaks at 13.02° disappeared, indicating the periodicity in the in-plane structure was partly lost. In addition, the peaks at 27.5° are gradually weakened, that may be because the deposition of AuNPs changed the interlayer distances. Simultaneously, five peaks appear at 38.2°, 44.4°, 64.8°, 77.7°, and 81.8°, respectively, corresponding to the (1 1 1), (2 0 0), (2 2 0), (3 1 1), and (2 2 2) lattice planes of Au (JCPDS 04-0784). No impure peaks were detected, indicating high purity of reduced AuNPs. The strongest peak at 38.2° reveals that (1 1 1) lattice plane is the primary orientation [49]. With the increase of Au loading amount, the diffraction peak heights of Au lattice planes are gradually increased and corresponding to the decrease in the width of these peaks, indicating an increase of Au crystallite size. The mean sizes of AuNPs are estimated by Scherrer–Debye equation with (1 1 1) peak as 8.2, 10.6, 14, and 19.3 nm for different concentration of $HAuCl_4$ treated PDA-g-C_3N_4.

The XPS of synthesized g-C_3N_4, PDA-g-C_3N_4, and PDA-g-C_3N_4/$Au_{(3)}$ are responsible for investigating the elements and chemical state of them. As shown in Fig. 3a, the survey spectra reveal the presence of same C, N, and O elements in g-C_3N_4 and PDA-g-C_3N_4 samples and Au in PDA-g-C_3N_4/$Au_{(3)}$. Compared with pure g-C_3N_4, there is a higher C and O percentage of PDA-g-C_3N_4 because PDA contains abundant oxygen-containing functional groups and less N content. In the high-resolution spectra for Au 4f and 4d, the Au $4f_{5/2}$, $4f_{7/2}$, $4d_{3/2}$, and $4d_{5/2}$ peaks are obviously located at 87.68, 83.98, 353.23 and 335.10 eV, which are typical values of Au in zero oxidation state (Fig. 3b–d). It verifies the successful

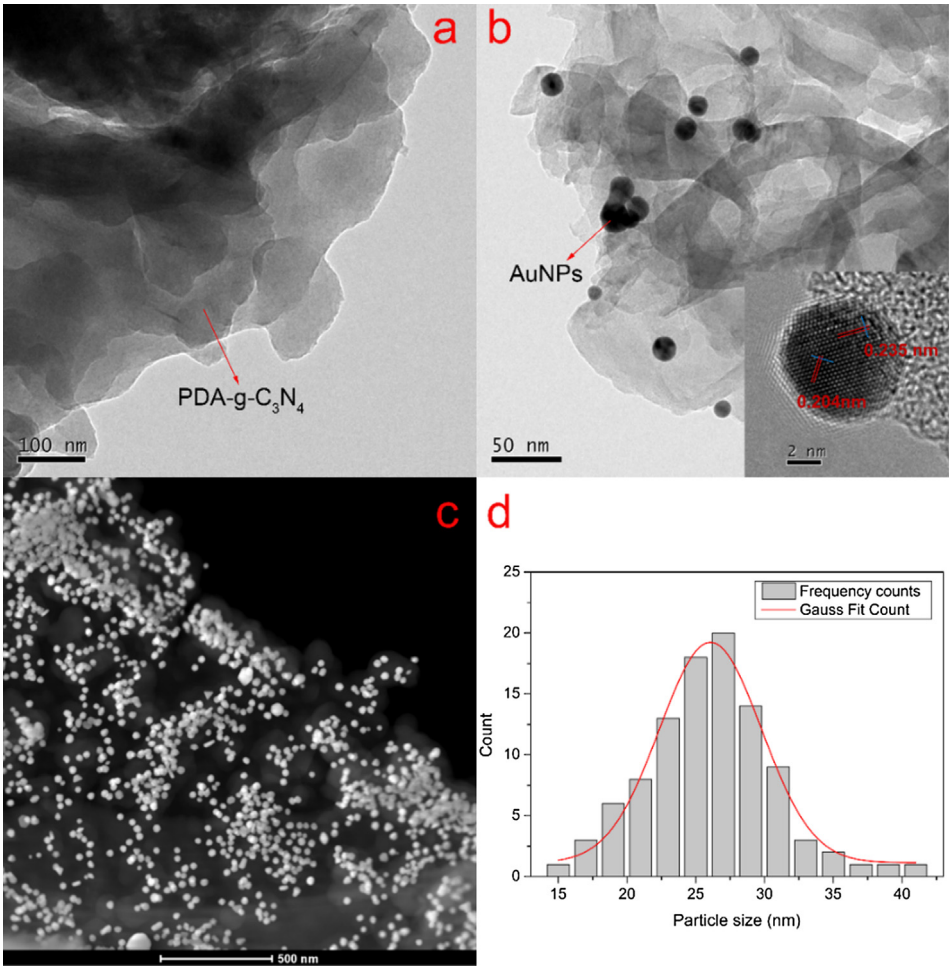

Fig. 1. TEM images of PDA-g-C_3N_4 support (a) and PDA-g-C_3N_4/$Au_{(3)}$ catalyst (b), STEM image (c) and histogram of Au particle size distribution of PDA-g-C_3N_4/$Au_{(3)}$ catalyst, insert of (b) is the HRTEM image.

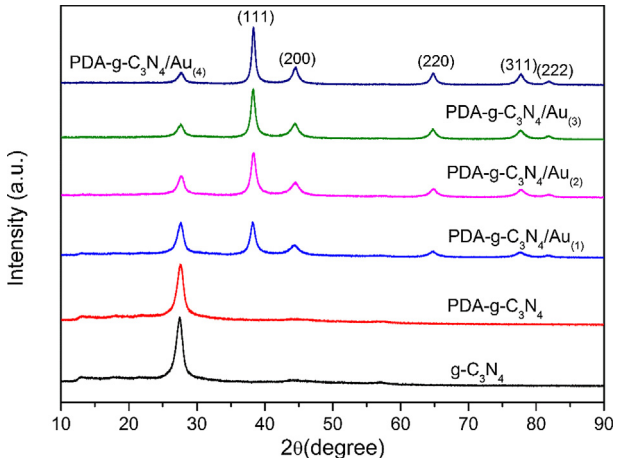

Fig. 2. XRD diffraction patterns of g-C_3N_4, PDA-g-C_3N_4, and different amount of Au loadings-based PDA-g-C_3N_4/Au.

reduction of AuNPs on the PDA-g-C_3N_4 surface, which is in good agreement with the XRD spectra and TEM images. The high-resolution spectra for C 1s, O 1s, and N 1s are presented in Fig. 4 (a–d), respectively. In the spectra of C 1s (Fig. 4a), pure g-C_3N_4 with two peaks at 285 and 288.4 eV is attributed to the alkyl carbon (C=C—C or C—H) and sp^2-bonded carbon (N—C—$(N)_2$) [18,50]. Besides, the sp^2-bonded carbon peak is the dominant peak due to the aromatic nitrogen heterocycle structure of g-C_3N_4. However, new peaks of C—O and C—N show in the PDA-g-C_3N_4 support which arises from PDA. This is owing to the rich hydroxyl and amino groups of PDA. In addition, after the loading of Au, the peaks of N—C—$(N)_2$, C—O, C—N, and C—C shift negatively which indicates that Au is successfully and tightly deposited on the support. In Fig. 4b, The increasing O content of PDA-g-C_3N_4 and PDA-g-C_3N_4/$Au_{(3)}$ is owing to the presence of PDA. For the O 1s spectrum of pure g-C_3N_4, the peaks at 531.7 and 533.3 eV are attributed to the adsorption of H_2O or CO_2 [51,52]. In PDA-g-C_3N_4, the peaks at 531 and 532.82 eV correspond to the O—C=O and C-O, respectively. In PDA-g-C_3N_4/$Au_{(3)}$, two peaks at 532 and 532.8 eV are attributed the adsorption of H_2O or CO_2 and C-O, respectively. In Fig. 4c, the N 1s spectrum of pure g-C_3N_4 can be separated into 3 peaks. The dominant peak at 398.83 eV is due to the sp^2-bonded nitrogen in triazine rings (C—N=C), and the peak at 400.6 eV is because of the bridging N atoms in N(—C)$_3$ or terminal amino groups (C—N—H) [53,54]. Particularly, an independent peak located at 404.6 eV becomes more obvious due to the protonation of g-C_3N_4, which causing CN heterocycles and cyano groups positively charged. This proves the prepared g-C_3N_4 is a nanosheet. The peaks of N(-C)$_3$ and C—N—H in PDA-g-C_3N_4 and PDA-g-C_3N_4/$Au_{(3)}$ become distinctly, and the peaks of C—N=C in them shift negatively. This is because the presence of PDA affects the concentration of C—N=C and the successful deposition of Au. Additionally, the peaks of PDA-g-C_3N_4 and PDA-g-C_3N_4/$Au_{(3)}$ at 404.6 eV are

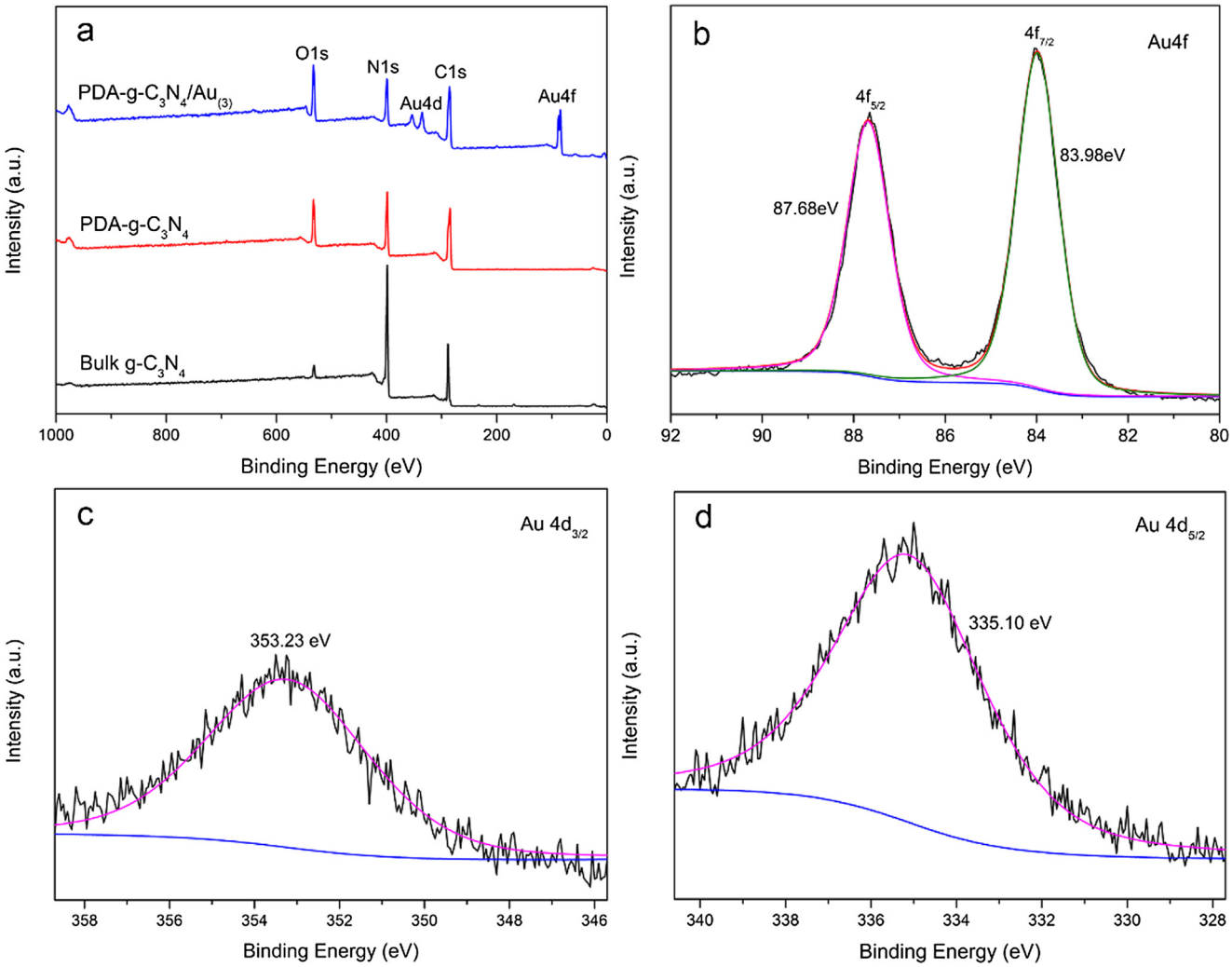

Fig. 3. XPS survey spectra (a) of g-C_3N_4, PDA-g-C_3N_4, and PDA-g-C_3N_4/$Au_{(3)}$, and high-resolution XPS spectra for Au 4f (b) and Au 4d (c-d) of PDA-g-C_3N_4/$Au_{(3)}$ catalyst.

lower than it in pure g-C_3N_4 which is because PDA and Au change the interlayer distances of g-C_3N_4 (Fig. 4d). This is well consistent with the results of XRD.

As exhibited in Fig. 5, the characteristic FT-IR spectra of g-C_3N_4, PDA-g-C_3N_4, and different amount of Au loadings-based PDA-g-C_3N_4/Au catalysts are similar and fewer differences, indicating that the original structure of g-C_3N_4 was maintained and the self-polymerization of DA and loading of AuNPs had few effects on the original structure of g-C_3N_4. For the spectrum of g-C_3N_4, the sharp peak at 806 cm^{-1} is accredited to the typical breathing mode of tri-s-triazine ring. After the coating of DA, the peak at 806 cm^{-1} is slight red shift to 808 cm^{-1} and the band intensity has slightly weakened, which demonstrate the successful self-polymerization of DA on g-C_3N_4 surface. In addition, the strong peaks from 1200 to 1650 cm^{-1} are the characteristic stretching band of CN heterocycles. The adsorption band located at 1640 cm^{-1} corresponds to the C-N stretching. The other three peaks at 1544, 1458, and 1403 cm^{-1} are related to the typical stretching vibration modes of C—N heterocycles. The bands located at about 1236 and 1317 cm^{-1} are attributed to either trigonal N(—C)$_3$ (full condensation) or bridging C-NH-C (partial condensation) [55]. The broad peaks in the region from 2800 to 3500 cm^{-1} are derived from the stretching vibration of N—H, as well as the physically adsorbed H_2O. In addition, different amounts of loaded AuNPs have little impact on the characteristic absorption peaks, because AuNPs do not show a characteristic absorption band in FT-IR spectrum [56].

3.2. Catalytic performance for reduction of nitroaromatics

3.2.1. Effecting parameters for nitroaromatics reduction

In order to investigate the effects on catalytic efficiency under different conditions, the concentration of $NaBH_4$ and dosage of catalyst were explored. $NaBH_4$ was used here to trigger the reduction reaction. When the catalyst added, there was no obvious color change and decrease of the absorption peak for 4-NP in the absence of $NaBH_4$. To further study the role of $NaBH_4$, different concentrations (10, 20, 40, 60, and 80 mM) of $NaBH_4$ were added. As shown in Fig. S2, the apparent rate constants (k_{app}) of the catalytic reaction for 4-NP are increased significantly until the concentration achieved 60 mM. Over this concentration, the catalytic rates are plateaued, this may be because the reactants are so saturated that even more $NaBH_4$ cannot further enhance the reaction rate. This phenomenon is similar to the result reported by Gupta at al. [57]. Thus, the $NaBH_4$ concentration of 60 mM was selected as the optimum concentration and used in all experiments. In order to investigate the effect of the dosage of catalyst, different amounts of catalyst in the range of 1–7 mg were used for 4-NP reduction (Fig. S3). In this respect, the catalytic rates of 4-NP reduction were increased with the increase of catalyst dosage basically. The increasing rate was most intensive from 4 mg to 5 mg, while it increased slowly after 5 mg. In order to balance the highest rate and minimum dosage of catalyst for the concept of economic friendly, 5 mg catalyst was used in the whole experiment.

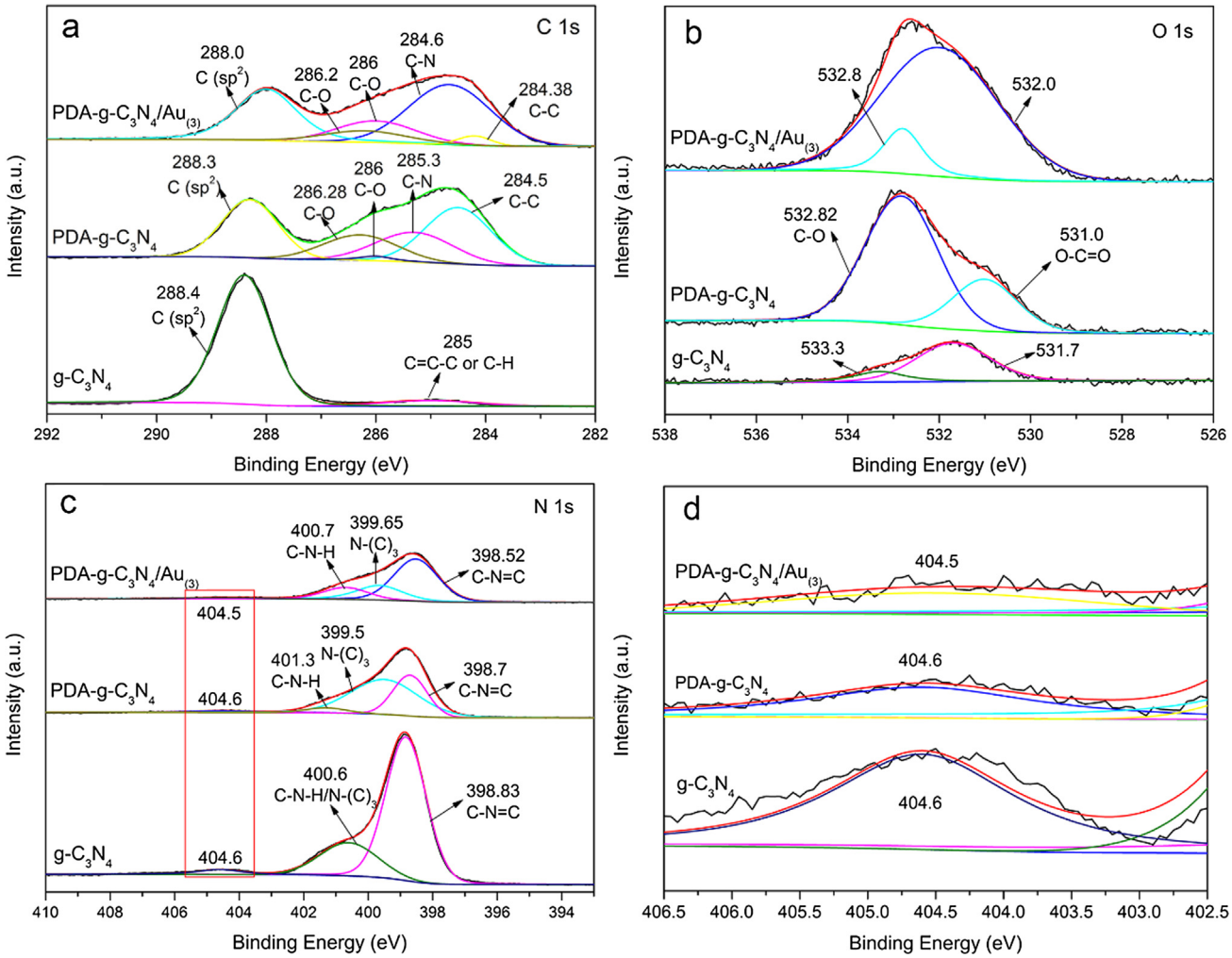

Fig. 4. High-resolution XPS spectra for C1s (a), O 1s (b), N 1s (c), amplifying N 1s from 402.5 to 406.5 eV (d) of g-C_3N_4, PDA-g-C_3N_4, and PDA-g-C_3N_4/$Au_{(3)}$.

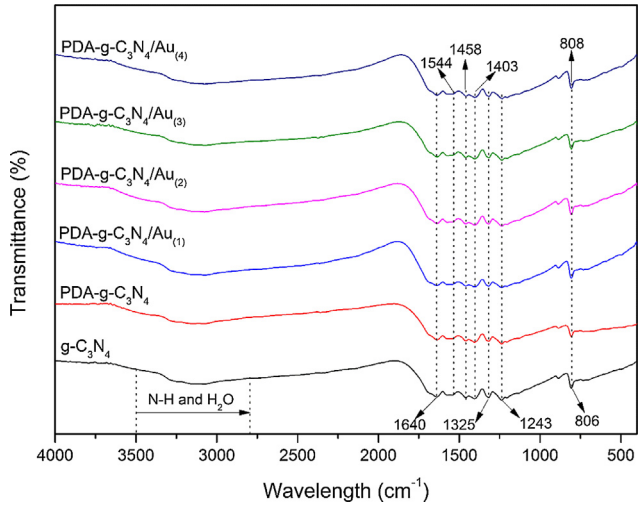

Fig. 5. The characteristic FT-IR spectra of g-C_3N_4, PDA-g-C_3N_4, and different amount of Au loadings-based PDA-g-C_3N_4/Au catalysts.

3.2.2. Catalytic reduction of 4-NP

The catalytic reduction of 4-NP with $NaBH_4$ was chosen as the model reaction to investigate the catalytic activity of as-prepared Au catalyst. Typically, a controlled experiment using the support (PDA-g-C_3N_4) was performed first. With the addition of $NaBH_4$, the color of 4-NP changed from light yellow to bright yellow (Insert of Fig. S4), which caused by the formation of 4-nitrophenolate ions [58]. The absorption peak of UV–Vis changed from 317 nm to 400 nm (Fig. S4). The absorption peak at 400 nm maintained stably all the time. As PDA-g-C_3N_4 added into the mixture solution, the absorption peak at 400 nm decreased slightly because of the weak adsorption of PDA-g-C_3N_4, while the peak near 298 nm corresponding to the product 4-AP [59] was not observed even over 1 h (Fig. S4). This indicates that the decrease of absorption peak at 400 nm was not induced by catalysis of PDA-g-C_3N_4, neither by $NaBH_4$. Conversely, as the catalyst with AuNPs, the intensity of absorption peak at 400 nm decreased obviously within few minutes (Fig. 6a). There was a new absorption peak at 298 nm corresponding to the production of 4-AP in the meantime. The successive intensity of 4-AP increased in sequence, similar with the previous reports [60,61]. However, it is different with the catalytic performance of Pt-based catalyst [62,63]. It could be because of the overlap of absorption peak between supports and 4-AP [42] or the different catalytic performance of Au- and Pt-based catalyst. In addition, different target contaminants, like o-nitroaniline, 2-NP, and CR etc., can lead to the similar result.

Since the concentration of $NaBH_4$ is a constant during catalytic reaction and much higher than 4-NP, the rate constants were evaluated by the pseudo-first-order kinetics. Typically, the ratios of respective absorbance (A_t/A_0) at 400 nm were measured to illustrate

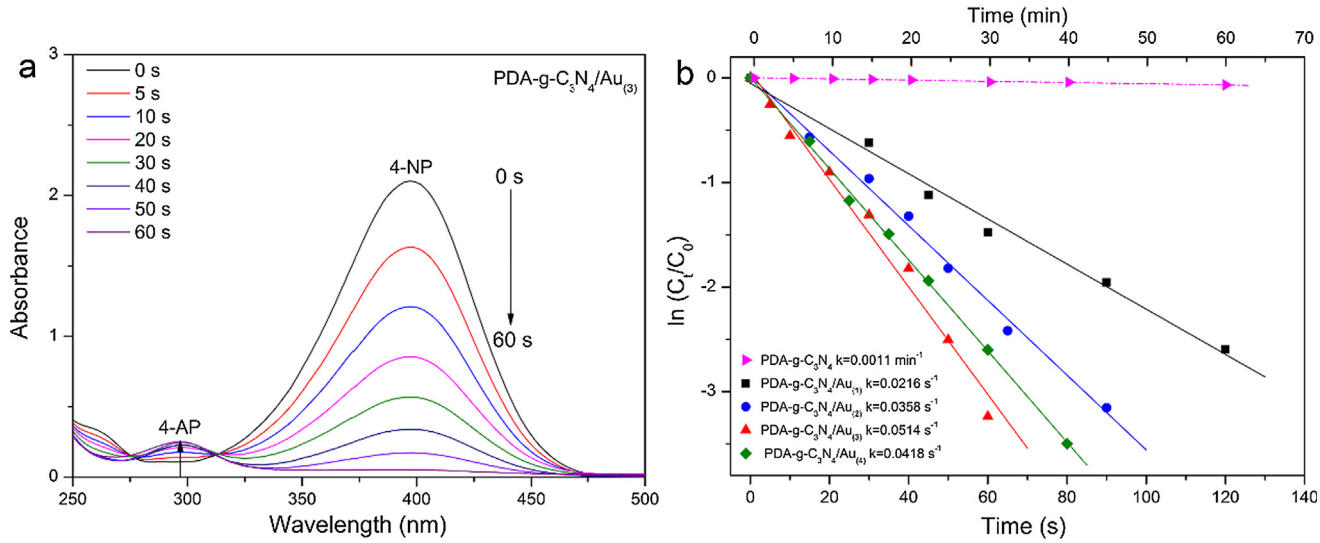

Fig. 6. Time-dependent UV–Vis absorption spectra of 4-NP reduced by PDA-g-C_3N_4/$Au_{(3)}$ catalyst (a). Plots of ln(C_t/C_0) versus reaction time for catalytic reduction of 4-NP by PDA-g-C_3N_4 and different PDA-g-C_3N_4/Au catalysts (b).

the ratios of C_t (concentration of 4-NP at time t) to C_0 (initial concentration of 4-NP). The linear relationship of ln(C_t/C_0) versus time (t) was showed and the rate constants k_{app} estimated directly by the slope of the straight line. It is reported that the catalytic efficiency of Au catalyst was highly related to the size and loading amount of AuNPs [64]. Therefore, the catalytic performance of different amounts of Au loadings were investigated. As shown in Fig. 6b, a good linear relationship of ln(C_t/C_0) versus t is observed for all Au-based catalysts, confirming the pseudo-first-order kinetics for this reaction. The rate constants k_{app} calculated are 0.0216, 0.0358, 0.0514, and 0.0418 s^{-1} for the reactions catalyzed by PDA-g-C_3N_4/$Au_{(1)}$, PDA-g-C_3N_4/$Au_{(2)}$, PDA-g-C_3N_4/$Au_{(3)}$, and PDA-g-C_3N_4/$Au_{(4)}$, respectively. The contents of Au performed by ICP-OES are 0.47%, 0.92%, 1.3%, and 1.87%. With the increase of Au loadings, the reduction of 4-NP was faster and the catalytic efficiency was enhanced. This is due to the increase of Au loadings provides more active sites, promoting the catalytic reaction. However, when the loadings of Au increased as 1.87%, the catalytic efficiency decreased. In order to explain this phenomenon, the TEM images of different Au catalysts were recorded (Fig. S5). With the amount of deposited AuNPs increasing, the shapes of AuNPs are more and more regular, although there are few other shapes of nano-Au production. Nevertheless, AuNPs tend to aggregate with the loading increased as 1.87%, which leads to the size of AuNPs increased significantly. In general, the decreasing particle size leads to an increase in the d-electron density of the Au atoms, which results in the increasing number of dissociatively adsorbed hydrogen atoms by AuNPs [65,66]. Thus, the AuNPs with smaller particles size are more effective than the larger ones. It is worth noting that the average sizes of deposited AuNPs in this work are gradually increasing, following the increased amount of AuNPs loadings. Therefore, the size and amount of AuNPs loadings play an important role in this work. Taking into consideration of the effect of Au loadings and dosage of the catalyst, the normalized rate constants, represented as k_{nor}, were calculated ($k_{nor} = k_{app}/m$, where m is the amount of Au catalysts). The results are shown in Table 1 and reveal that the catalytic efficiency of PDA-g-C_3N_4/$Au_{(3)}$ is much higher than others, 4-NP can be reduced within 60 s by PDA-g-C_3N_4/$Au_{(3)}$. The k_{app} (0.0514 s^{-1}) and k_{nor} (10.28 s^{-1} g^{-1}) are nearly 9 and 1.7 times higher than that of Au/g-C_3N_4 catalyst (5.9362×10^{-3} s^{-1} and 5.9362 s^{-1} g^{-1}), respectively [29]. For heterogeneous catalysis, the turnover frequency (TOF) of catalyst is important for evaluating the catalytic efficiency. In general, TOF is defined as the number of passes through the catalytic cycles per unit time, which is calculated by the moles of 4-NP reduced per mole of Au per hour. As summarized in Table 1, the TOF of PDA-g-C_3N_4/$Au_{(3)}$ is higher than the others. Therefore, although the average size of PDA-g-C_3N_4/$Au_{(3)}$ is larger than PDA-g-C_3N_4/$Au_{(1)}$ and PDA-g-C_3N_4/$Au_{(2)}$, the catalytic efficiency is still higher because of the large amount of Au loadings. In addition, the catalytic activity of PDA-g-C_3N_4/$Au_{(3)}$ and other Au catalytic systems even other novel metal-based systems are compared (Table 2). Compared with other catalytic systems, the catalytic activity of PDA-g-C_3N_4/$Au_{(3)}$ is high, but the size of AuNPs is much larger than others. This is may be because the strong reduction ability of PDA and good synergistic effect between PDA-g-C_3N_4 and AuNPs, which deposited large amount of AuNPs on the surface and accelerated the catalytic performance of PDA-g-C_3N_4/$Au_{(3)}$, respectively. On the basis of large size of PDA-g-C_3N_4/$Au_{(3)}$, the catalytic performance of this Au catalyst is generally satisfactory when comparing with other systems.

3.2.3. Catalytic reduction of other nitroaromatics

In order to illustrate the catalytic activity of prepared Au catalyst, the reduction of other nitroaromatics including 2-NP, 2, 4-DNP, MO, CR, and EBT were investigated. When catalysts added, these nitroaromatics became colorless in few minutes (Fig. S6). The time-dependent reduction of them under the same condition of 4-NP reduction is summarized in Fig. 7. The results show the reduction rate followed the order of MO > 4-NP > 2-NP > 2, 4-DNP > EBT > CR. A common kinetic profile reveals that these compounds were largely reduced in few seconds, after which reduction slowed, possibly, owing to the reduced amount of reactants remaining in the system. The order of 4-NP > 2-NP > 2, 4-DNP is highly consistent with the reported paper [42]. As reported by Xia et al. [74], the reduction of nitrophenols by $NaBH_4$ may be related to the conjugation effect, inductive effect and/or molecular orientation of the group on the nitrophenols. Theoretically, 4-NP and 2-NP may be stable because the conjugation effect transfers the negative charge into nitro group. In addition, the distance between —NO_2 and —OH in 4-NP is higher than that in 2-NP. That is to say, weaker inductive effect results in less positively charged nitrogen atom in 4-NP. However, the reduction catalysis of nitrophenols by $NaBH_4$ starts from the attack against nitrogen atom of

Table 1
Summary of the reaction time (t), conversion (%), apparent rate constant (k_{app}), normalized apparent rate constant (k_{nor}), and TOF (h^{-1}) for different catalysts at room temperature.

Catalyst	Reaction time (s)	Conversion (%)	k_{app} (s^{-1})	k_{nor} (s^{-1} g^{-1})	TOF (h^{-1})
PDA-g-C_3N_4/$Au_{(1)}$	150	80	0.0216	4.32	482.85
PDA-g-C_3N_4/$Au_{(2)}$	90	95	0.0358	7.16	513.91
PDA-g-C_3N_4/$Au_{(3)}$	60	100	0.0514	10.28	545.60
PDA-g-C_3N_4/$Au_{(4)}$	80	100	0.0418	8.36	284.44

Table 2
Comparison for the catalytic performances of PDA-g-C_3N_4/$Au_{(3)}$ with other catalyst systems over 4-NP reduction.

Catalyst	Catalyst mass (mg)	Particle size (nm)	k_{app} (10^{-3} s^{-1})	k_{nor} (s^{-1} g^{-1})	Cycles	Ref.
Fe_3O_4@PDA–Au_6	0.05	–	10.5	210	8	[44]
Pt3Au1-PDA/RGO[a]	0.06	0.407	9.58	160	6	[42]
Au@g-C_3N_4-PANI[b]	1	10	8.39	8.39	5	[67]
Au/g-C_3N_4-6	1	2.6	5.94	5.94	10	[29]
AuNPs	–	25	0.445	–	–	[68]
AuNPs	1.46×10^{-3} mol	29	9.83	6.73 (s^{-1} mol^{-1})	–	[46]
AuNP-5	0.0052	2	26.3	5057.69	–	[69]
RGO-PMS[c]@AuNPs	0.8	10	15.01	18.76	–	[70]
Au@CMK-3-O[d]	75	10	7.75	0.1	6	[71]
AC[e]/Au	–	4	16.7	–	–	[72]
Au@PZS[f]@CNTs[g]	0.3	6	1.78	5.93	6	[73]
$Ni_{0.22}$/CB[h]	1	22.5	9.95	9.95	10	[74]
AgNPs/SNTs[i]-4	5	2.85	38.41	7.68	–	[75]
$Cu_{54}Ni_{46}$@SiO_2	5	5.7 ± 0.5	5.10	1.02	10	[76]
PdAu/Fe_3O_4	1.1	–	5.47	4.84	8	[77]
PDA-g-C_3N_4/$Au_{(3)}$	5	26.1	51.4	10.28	10	This work

[a] RGO, reduced graphene oxide.
[b] PANI polyaniline.
[c] PMS, periodic mesoporous silica.
[d] CMK-3-O, oxidized mesoporous carbon.
[e] AC, activated carbon.
[f] PZS, Poly(cyclotriphosphazene-*co*-4,4′-sulfonyldiphenol).
[g] CNTs, carbon nanotubes.
[h] CB, carbon black.
[i] SNTs, silica nanotubes.

—NO_2 by negatively charged active hydrogen. Thus, 4-NP with less positively charged nitrogen atom should have lower reactivity [78]. On the contrary, reduction of 4-NP exhibits higher activity than that of 2-NP. This is possibly because the steric effect plays a main role among all of these effects. Among the three nitrophenols, 2,4-DNP shows the lowest reactivity because of two —NO_2 groups. Generally, the reduction activity of simple nitrophenol is higher than that of complicated azo dyes because the reaction process of azo dyes is more complex [44]. Interestingly, in this work, the reduction efficiency of MO is much higher than other nitroaromatics, even simple nitrophenols. This may be relative to the route of dyes reduction. As reported by Haber in 1898, the reduction of nitrophenols could be divided into two probable routes: the condensation and direct routes [79]. As described by the condensation route, the azo groups were attacked by activation hydrogen to form hydrazo groups, and finally became aniline compounds. This route is fast and simple and is the possible route for MO reduction because MO only contains one azo group (Fig. S7). Thus, it is reasonable that the catalytic activity of MO is higher than the others. As for EBT and CR, they do not only have nitro or azo group alone, but contain nitro and azo group both or two azo groups respectively. The reduction of them needs more time and more activation hydrogen, hence the catalytic activities of them are lower.

3.3. Mechanistic insight in the reduction of 4-NP by PDA-g-C_3N_4/Au system

The PDA anchoring on g-C_3N_4 is a biopolymer with abundant amine and catechol groups, which can help to reduce and stabilize AuNPs [80]. As shown in Scheme 1a, PDA with good stability is auto-polymerized on the surface of g-C_3N_4 to form the PDA-g-C_3N_4 support. After the addition of $HAuCl_4$, AuNPs are successfully reduced by PDA and well-dispersed on the surface of the support. Because of the excess of $NaBH_4$ and the kinetic studies in this work, the mechanism for the reduction of 4-NP by as-prepared Au catalyst is proposed based on the Langmuir–Hinshelwood mechanism [81,82]. Zero-order kinetic process occurs considering the rate determining steps and the heterogeneous catalysis reaction can be divided into six steps: (1) the adsorption of targets (4-NP) to PDA-g-C_3N_4/Au catalyst, (2) diffusion of these compounds to the surface of Au active sites, (3) reaction of borohydride ions (BH_4^-) with water to form metaborate (BO_2^-) and activation hydrogen (H_2), (4) formation of the reactive Au-H species and hydride transfer from Au-H species to the targets, (5) reduction of the target compounds to form the adsorbed products (4-AP), and (6) eventually desorption of products from the surface of catalyst. In this process, a series of electron transfer processes play the major role on the critical rate-limiting step. In addition, high deposition and dispersity of AuNPs provide much active sites for bonding with H_2 and promote the electron transfer. With the presence of Au-H species, the nitro group of 4-NP is first reduced to nitroso group, and then turns into hydroxylamine fast. Finally, the corresponding 4-AP is generated in the rate determining step (Scheme 1b). The high activity of PDA-g-C_3N_4/$Au_{(3)}$ may be attributed to the high deposition and dispersity of AuNPs and specific properties of catalyst. Abundant amino groups and N-containing structure of g-C_3N_4 provide good compatibility with PDA and AuNPs and possess strong H^+ adsorption ability [30,83]. It is benefit for the adsorption of 4-NP, which provides higher concentration of 4-NP near to AuNPs, inducing highly efficient contact between 4-NP and the active sites.

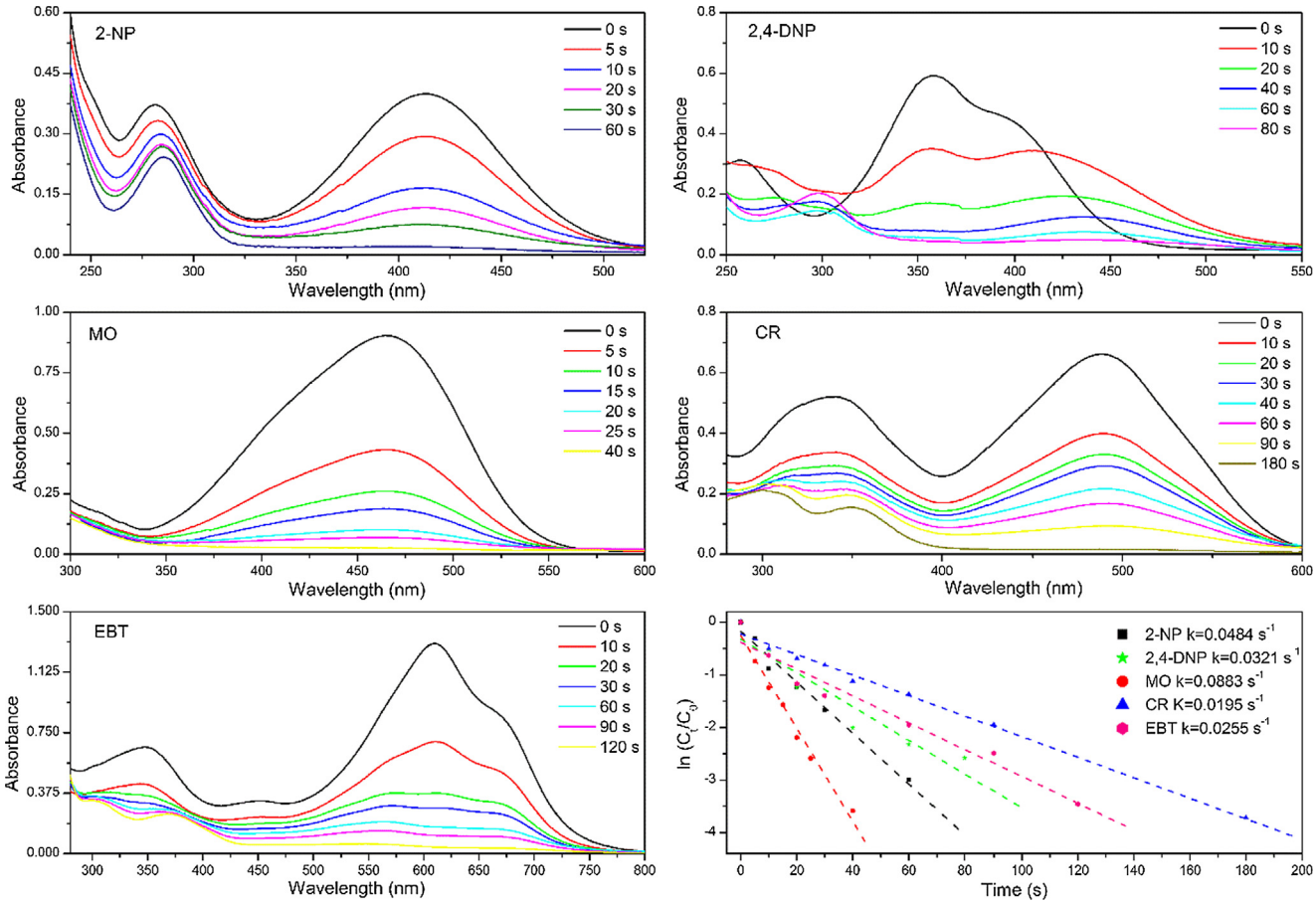

Fig. 7. Time-dependent UV–Vis absorption spectra and plots of $\ln(C_t/C_0)$ versus reaction time of 2-NP, 2, 4-DNP, MO, CR, and EBT reduced by PDA-g-C_3N_4/$Au_{(3)}$ catalyst.

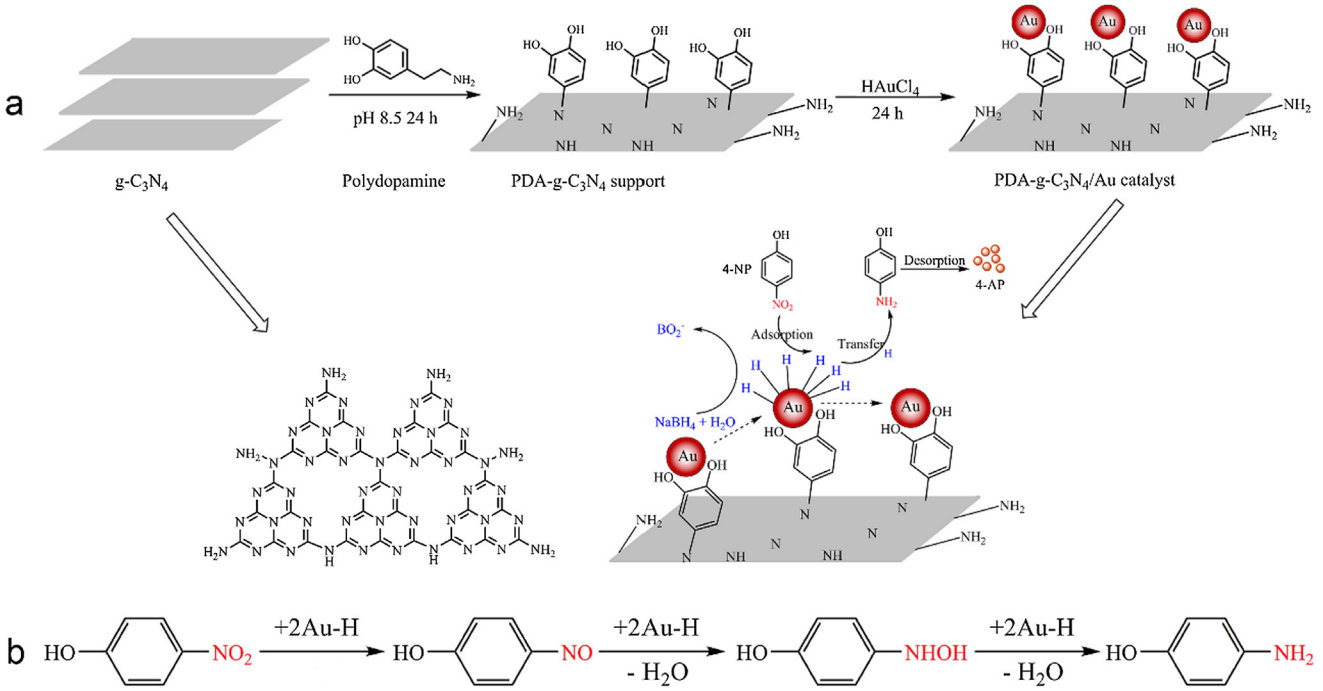

Scheme 1. Mechanism of PDA-g-C_3N_4/Au synthesis and catalytic reduction of 4-NP (a). Reaction route for reduction of 4-NP to 4-AP by PDA-g-C_3N_4/Au (b).

3.4. Recycle and practical application

To investigate the stability and reusability, the PDA-g-C_3N_4/$Au_{(3)}$ catalyst with the highest catalytic activity was used to reduce 4-NP over ten cycles. As exhibited in Fig. 8, the PDA-g-C_3N_4/$Au_{(3)}$ catalyst not only shows a comparable stability after several recycles, but also reveals a high reducing efficiency for 4-NP reduction, and only slight decay after 10 recycles. One of the important problems for the supported Au catalyst is the leaching of Au, thus the amount of Au in the aqueous phase after the reaction was measured by ICP-OES. The results reveal that there is almost no Au leaching in the first few times. After several times recycles, the presence of Au in percentages corresponding to 0.7, 0.5, 0.4, and 0.2% of the initial Au content of PDA-g-C_3N_4/$Au_{(3)}$. The results indicate that the leaching of Au is very low and is negligible for the influence of environment.

The catalytic performance of PDA-g-C_3N_4/$Au_{(3)}$ on real water was proposed. The UV–Vis spectra of bottled water, tap water, river water, and lake water indicated that there were no 4-NP in them. After the spiking of standard 4-NP solution, the colors all changed from light yellow to bright yellow and were brighter than 4-NP in ultrapure water except bottled water. Besides, the tap water, river water, and lake water samples were much brighter than the other one (insert of Fig. 9a). After mixed with $NaBH_4$, the color of these samples was in accordance with the ultrapure water sample. To explore the causes of this phenomenon, the pH and UV–Vis spectra were measured. The pH of bottled water, tap water, river water, and lake water was 8.03, 7.57, 7.72, and 7.99, respectively. As shown in the UV–Vis spectra (Fig. 9a), the absorption peaks of 4-NP in tap water, river water, and lake water samples occur at 400 nm and the intensities are different, which suggests that 4-NP turns into 4-nitrophenolate ions partly. Possible reasons are that (1) the alkaline environment drives the formation of 4-nitrophenolate ions; (2) there are some substances in these water samples and play the role like $NaBH_4$, which induces the formation of 4-nitrophenolate ions. Based on this, the reduction experiment of these four samples without $NaBH_4$ was proposed. Results showed that there were no new absorption peaks appeared near 298 nm, demonstrating these substances played a role of promoting the formation of 4-nitrophenolate ions, rather than trigger the catalytic reaction. When mixing with $NaBH_4$ and after the addition of PDA-g-C_3N_4/$Au_{(3)}$ catalyst, the color of bottled water, tap water, river water, and lake water samples turned into colorless in few minutes. New absorption peaks of UV–Vis for them occur near 298 nm, which reveals the product of 4-AP (Fig. S8). The rate constants k_{app} are calculated at 0.0407, 0.0267, 0.0486, and 0.0815 s^{-1}, respectively. The catalytic efficiency of tap water is obviously lower than the others. This maybe because that the presence of a large number of Cl^- ions is toxic to Au catalyst, which can inhibit the catalytic activity by poisoning the active site [84]. Interestingly, the catalytic efficiency of lake water sample is much higher than the others, and we speculate this may be related to the initial formation of higher concentration of 4-nitrophenolate ions and the presence of substance such as dissolved oxygen (DO) in other waters may consume $NaBH_4$ which decreases the catalytic reaction. Thus, the concentration of DO in different water samples were further measured at room temperature. And the results showed that the concentration of DO in bottled water, tap water, river water, and lake water were 6.25, 6.51, 6.32, and 3.70 mg L^{-1}, respectively. There were much lower concentration of DO in lake water, resulting in more $NaBH_4$ acted on the reduction reaction. Hence, the catalytic activity of PDA-g-C_3N_4/Au in lake water is higher than the others. In general, the PDA-g-C_3N_4/Au can be used

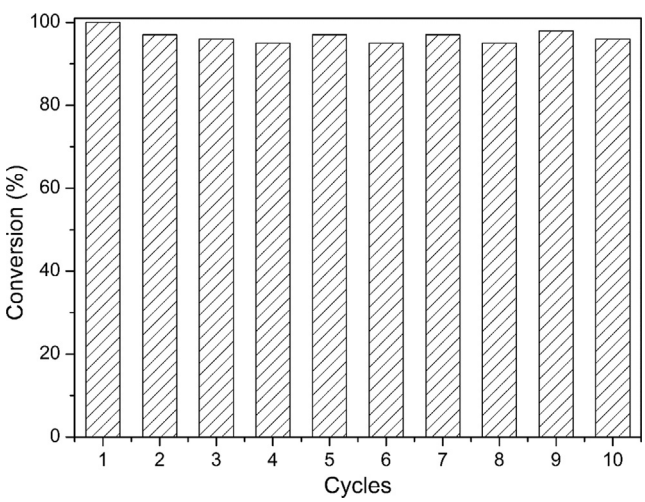

Fig. 8. Reusability of 4-NP reduction by PDA-g-C_3N_4/$Au_{(3)}$ catalyst for 5 min over ten cycles.

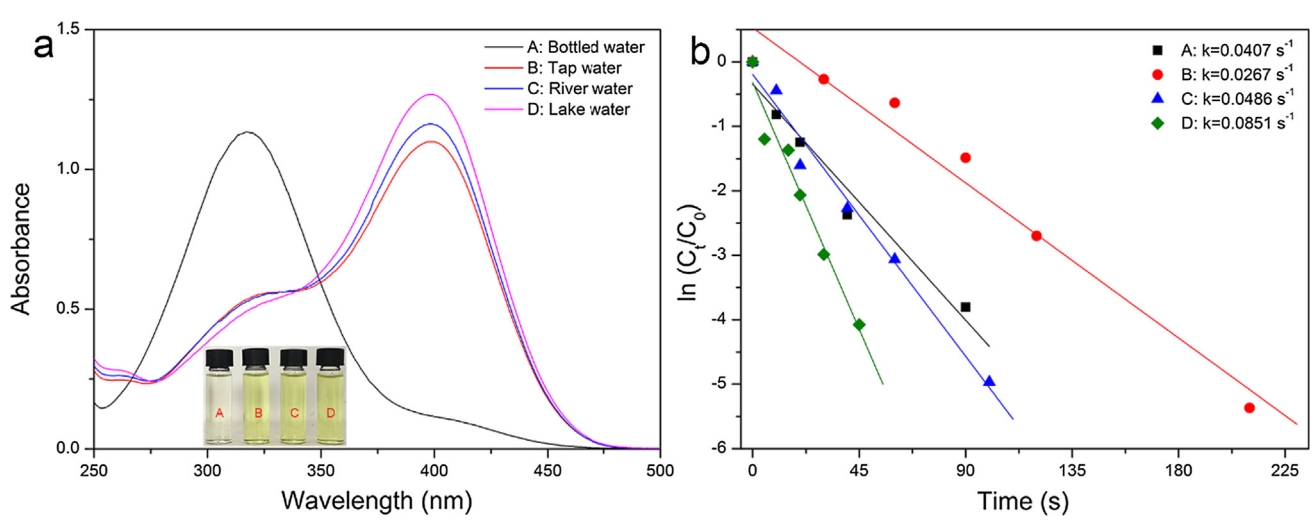

Fig. 9. Time-dependent UV–Vis absorption spectra and photograph (insert) of 4-NP in different real water samples (a) and plot of $\ln(C_t/C_0)$ versus reaction time of 4-NP reduction by PDA-g-C_3N_4/$Au_{(3)}$ catalyst in different real water samples (b). (A-D represent the real samples of bottled water, tap water, river water, and lake water, respectively.)

as a promising catalyst for environmental water purification in practical application.

4. Conclusion

In this work, a facile in-situ method for different Au loadings of PDA-g-C_3N_4 catalyst has been successfully reported. In this procedure, PDA acts as both the reductant and stabilizer of AuNPs. With the increase of Au loadings, the catalytic efficiency increases and PDA-g-$C_3N_4/Au_{(3)}$ has shown good catalytic activity towards the reduction of 4-NP with a high k_{app} of 0.0514 s^{-1}. The PDA-g-$C_3N_4/Au_{(3)}$ also exhibits satisfactory catalytic performance of other nitroaromatics including 2-NP, 2, 4-DNP, MO, CR, and EBT and the reduction rate follows the order of MO > 4-NP > 2-NP > 2, 4-DNP > EBT > CR. The high activity of this catalyst is ascribed to the high deposition and dispersity of AuNPs and the specific properties of catalyst. In addition, the support of PDA-g-C_3N_4 has been proven to can be a good photocatalytic candidate for contaminant degradation and hydrogen evolution [85,86]. Coincidentally, AuNPs is one of great photocatalytic adjuvants. It can be the antennas for the visible light absorption, sensor for electron transfer, and electron sink for electrons trapping because of the extraordinary surface plasmon resonance properties and remarkable photostability [87,88]. Thus, this simple and green synthetic PDA-g-C_3N_4/Au catalyst not only can guide the fabrication of other nanocatalysts, but also can be used in reduction and photocatalytic fields respectively for different purposes.

Acknowledgments

This study was financially supported by the Program for the National Natural Science Foundation of China (51579098, 51779090, 51709101, 51278176, 51408206, 51521006), Science and Technology Plan Project of Hunan Province (2016RS3026, 2017SK2243), the National Program for Support of Top-Notch Young Professionals of China (2014), the Program for New Century Excellent Talents in University (NCET-13-0186), the Program for Changjiang Scholars and Innovative Research Team in University (IRT-13R17), and the Fundamental Research Funds for the Central Universities (531107050978, 531107051080).

Appendix A. Supplementary material

Supplementary data to this article can be found online at https://doi.org/10.1016/j.jcis.2018.09.051.

References

[1] D. Sebastián, A.G. Ruíz, I. Suelves, R. Moliner, M.J. Lázaro, V. Baglio, A. Stassi, A. S. Aricò, Enhanced oxygen reduction activity and durability of Pt catalysts supported on carbon nanofibers, Appl. Catal. B 115 (2012) 269–275.
[2] J. Shen, Y. Zhou, J. Huang, Y. Zhu, J. Zhu, X. Yang, W. Chen, Y. Yao, S. Qian, H. Jiang, C. Li, In-situ SERS monitoring of reaction catalyzed by multifunctional Fe_3O_4@TiO_2@Ag-Au microspheres, Appl. Catal. B 205 (2017) 11–18.
[3] D. Vidyasagar, S.G. Ghugal, A. Kulkarni, P. Mishra, A.G. Shende, S.S. Jagannath, S. S. Umare, R. Sasikala, Silver/Silver(II) oxide (Ag/AgO) loaded graphitic carbon nitride microspheres: an effective visible light active photocatalyst for degradation of acidic dyes and bacterial inactivation, Appl. Catal. B 221 (2018) 339–348.
[4] X. Yang, P.-F. Tian, C. Zhang, Y.-Q. Deng, J. Xu, J. Gong, Y.-F. Han, Au/carbon as Fenton-like catalysts for the oxidative degradation of bisphenol A, Appl. Catal. B 134 (2013) 145–152.
[5] L. Wang, E. Guan, J. Zhang, J. Yang, Y. Zhu, Y. Han, M. Yang, C. Cen, G. Fu, B.C. Gates, Single-site catalyst promoters accelerate metal-catalyzed nitroarene hydrogenation, Nat. Commun. 9 (2018) 1362.
[6] I.X. Green, W. Tang, M. Neurock, J.T. Yates, Spectroscopic observation of dual catalytic sites during oxidation of CO on a Au/TiO_2 catalyst, Science 333 (2011) 736–739.
[7] D. Preti, C. Resta, S. Squarcialupi, G. Fachinetti, Carbon dioxide hydrogenation to formic acid by using a heterogeneous gold catalyst, Angew. Chem. Int. Ed. 50 (2011) 12551–12554.
[8] X. Tan, Y. Liu, G. Zeng, X. Wang, X. Hu, Y. Gu, Z. Yang, Application of biochar for the removal of pollutants from aqueous solutions, Chemosphere 125 (2015) 70–85.
[9] F. Long, J.L. Gong, G.M. Zeng, L. Chen, X.Y. Wang, J.H. Deng, Q.Y. Niu, H.Y. Zhang, X.R. Zhang, Removal of phosphate from aqueous solution by magnetic Fe–Zr binary oxide, Chem. Eng. J. 171 (2011) 448–455.
[10] P. Xu, G.M. Zeng, D.L. Huang, C. Lai, M.H. Zhao, Z. Wei, N.J. Li, C. Huang, G.X. Xie, Adsorption of Pb (II) by iron oxide nanoparticles immobilized Phanerochaete chrysosporium: equilibrium, kinetic, thermodynamic and mechanisms analysis, Chem. Eng. J. 203 (2012) 423–431.
[11] M. Chen, P. Xu, G. Zeng, C. Yang, D. Huang, J. Zhang, Bioremediation of soils contaminated with polycyclic aromatic hydrocarbons, petroleum, pesticides, chlorophenols and heavy metals by composting: applications, microbes and future research needs, Biotechnol. Adv. 33 (2015) 745–755.
[12] P. Zhao, X. Feng, D. Huang, G. Yang, D. Astruc, Basic concepts and recent advances in nitrophenol reduction by gold-and other transition metal nanoparticles, Coord. Chem. Rev. 287 (2015) 114–136.
[13] P. Xu, G.M. Zeng, D.L. Huang, C.L. Feng, S. Hu, M.H. Zhao, C. Lai, Z. Wei, C. Huang, G.X. Xie, Use of iron oxide nanomaterials in wastewater treatment: a review, Sci. Total Environ. 424 (2012) 1–10.
[14] S. Wang, J. Wang, Q. Zhao, D. Li, J.-Q. Wang, M. Cho, H. Cho, O. Terasaki, S. Chen, Y. Wan, Highly active heterogeneous 3 nm gold nanoparticles on mesoporous carbon as catalysts for low-temperature selective oxidation and reduction in water, ACS Catal. 5 (2015) 797–802.
[15] R. Pocklanova, A.K. Rathi, M.B. Gawande, K.K.R. Datta, V. Ranc, K. Cepe, M. Petr, R.S. Varma, L. Kvitek, R. Zboril, Gold nanoparticle-decorated graphene oxide: synthesis and application in oxidation reactions under benign conditions, J. Mol. Catal. A: Chem. 424 (2016) 121–127.
[16] K.S. Novoselov, A.K. Geim, S.V. Morozov, D. Jiang, Y. Zhang, S.V. Dubonos, I.V. Grigorieva, A.A. Firsov, Electric field effect in atomically thin carbon films, Science 306 (2004) 666.
[17] H. Liu, J. Wang, Z. Feng, Y. Lin, L. Zhang, D. Su, Facile synthesis of Au nanoparticles embedded in an ultrathin hollow graphene nanoshell with robust catalytic performance, Small 11 (2015) 5059–5064.
[18] C. Zhou, C. Lai, D. Huang, G. Zeng, C. Zhang, M. Cheng, L. Hu, J. Wan, W. Xiong, M. Wen, X. Wen, L. Qin, Highly porous carbon nitride by supramolecular preassembly of monomers for photocatalytic removal of sulfamethazine under visible light driven, Appl. Catal. B 220 (2018) 202–210.
[19] W.-W. Tang, G.-M. Zeng, J.-L. Gong, J. Liang, P. Xu, C. Zhang, B.-B. Huang, Impact of humic/fulvic acid on the removal of heavy metals from aqueous solutions using nanomaterials: a review, Sci. Total Environ. 468 (2014) 1014–1027.
[20] J.H. Deng, X.R. Zhang, G.M. Zeng, J.L. Gong, Q.Y. Niu, J. Liang, Simultaneous removal of Cd(II) and ionic dyes from aqueous solution using magnetic graphene oxide nanocomposite as an adsorbent, Chem. Eng. J. 226 (2013) 189–200.
[21] M.Q. Wen, T. Xiong, Z.G. Zang, W. Wei, X.S. Tang, F. Dong, Synthesis of MoS_2/g-C_3N_4 nanocomposites with enhanced visible-light photocatalytic activity for the removal of nitric oxide (NO), Opt. Express 24 (2016) 10205–10212.
[22] B. Vellaichamy, P. Periakaruppan, Catalytic hydrogenation performance of an in situ assembled Au@g-C_3N_4–PANI nanoblend: synergistic inter-constituent interactions boost the catalysis, New J. Chem. 41 (2017) 7123–7132.
[23] X.-H. Li, X. Wang, M. Antonietti, Mesoporous g-C_3N_4 nanorods as multifunctional supports of ultrafine metal nanoparticles: hydrogen generation from water and reduction of nitrophenol with tandem catalysis in one step, Chem. Sci. 3 (2012) 2170–2174.
[24] M. Boronat, A. Corma, F. Illas, J. Radilla, T. Ródenas, M.J. Sabater, Mechanism of selective alcohol oxidation to aldehydes on gold catalysts: influence of surface roughness on reactivity, J. Catal. 278 (2011) 50–58.
[25] J.-L. Gong, B. Wang, G.-M. Zeng, C.-P. Yang, C.-G. Niu, Q.-Y. Niu, W.-J. Zhou, Y. Liang, Removal of cationic dyes from aqueous solution using magnetic multi-wall carbon nanotube nanocomposite as adsorbent, J. Hazard. Mater. 164 (2009) 1517–1522.
[26] C. Zhang, C. Lai, G. Zeng, D. Huang, C. Yang, Y. Wang, Y. Zhou, M. Cheng, Efficacy of carbonaceous nanocomposites for sorbing ionizable antibiotic sulfamethazine from aqueous solution, Water Res. 95 (2016) 103–112.
[27] Y. Zhang, G.M. Zeng, L. Tang, J. Chen, Y. Zhu, X.X. He, Y. He, Electrochemical sensor based on electrodeposited graphene-Au modified electrode and nanoAu carrier amplified signal strategy for attomolar mercury detection, Anal. Chem. 87 (2015) 989–996.
[28] Z. Wang, K. Dong, Z. Liu, Y. Zhang, Z. Chen, H. Sun, J. Ren, X. Qu, Activation of biologically relevant levels of reactive oxygen species by Au/g-C_3N_4 hybrid nanozyme for bacteria killing and wound disinfection, Biomaterials 113 (2017) 145–157.
[29] Y. Fu, T. Huang, B. Jia, J. Zhu, X. Wang, Reduction of nitrophenols to aminophenols under concerted catalysis by Au/g-C_3N_4 contact system, Appl. Catal. B 202 (2017) 430–437.
[30] X. Guo, F. Wu, Y. Ni, S. Kokot, Synthesizing a nano-composite of BSA-capped Au nanoclusters/graphitic carbon nitride nanosheets as a new fluorescent probe for dopamine detection, Anal. Chim. Acta 942 (2016) 112–120.
[31] J. Liang, Z. Yang, L. Tang, G. Zeng, M. Yu, X. Li, H. Wu, Y. Qian, X. Li, Y. Luo, Changes in heavy metal mobility and availability from contaminated wetland soil remediated with combined biochar-compost, Chemosphere 181 (2017) 281–288.
[32] H. Wu, C. Lai, G. Zeng, J. Liang, J. Chen, J. Xu, J. Dai, X. Li, J. Liu, M. Chen, The interactions of composting and biochar and their implications for soil

amendment and pollution remediation: a review, Crit. Rev. Biotechnol. 37 (2017) 754–764.
[33] L. Qin, G. Zeng, C. Lai, D. Huang, P. Xu, C. Zhang, M. Cheng, X. Liu, S. Liu, B. Li, "Gold rush" in modern science: fabrication strategies and typical advanced applications of gold nanoparticles in sensing, Coord. Chem. Rev. 359 (2018) 1–31.
[34] L. Qin, G. Zeng, C. Lai, D. Huang, C. Zhang, P. Xu, T. Hu, X. Liu, M. Cheng, Y. Liu, A visual application of gold nanoparticles: simple, reliable and sensitive detection of kanamycin based on hydrogen-bonding recognition, Sens. Actuat. B. 243 (2017) 946–954.
[35] M. Haruta, Size- and support-dependency in the catalysis of gold, Catal. Today 36 (1997) 153–166.
[36] G. Shi, Y. Li, G. Xi, Q. Xu, Z. He, Y. Liu, J. Zhang, J. Cai, Rapid green synthesis of gold nanocatalyst for high-efficiency degradation of quinclorac, J. Hazard. Mater. 335 (2017) 170–177.
[37] F. He, G. Chen, Y. Yu, Y. Zhou, Y. Zheng, S. Hao, The synthesis of condensed C-PDA-g-C_3N_4 composites with superior photocatalytic performance, Chem. Commun. 51 (2015) 6824–6827.
[38] H. Lee, S.M. Dellatore, W.M. Miller, P.B. Messersmith, Mussel-inspired surface chemistry for multifunctional coatings, Science 318 (2007) 426–430.
[39] Y. Lee, T.G. Park, Facile fabrication of branched gold nanoparticles by reductive hydroxyphenol derivatives, Langmuir 27 (2011) 2965–2971.
[40] B. Fei, B. Qian, Z. Yang, R. Wang, W. Liu, C. Mak, J.H. Xin, Coating carbon nanotubes by spontaneous oxidative polymerization of dopamine, Carbon 46 (2008) 1795–1797.
[41] K.C. Black, Z. Liu, P.B. Messersmith, Catechol redox induced formation of metal core– polymer shell nanoparticles, Chem. Mater. 23 (2011) 1130–1135.
[42] W. Ye, J. Yu, Y. Zhou, D. Gao, D. Wang, C. Wang, D. Xue, Green synthesis of Pt–Au dendrimer-like nanoparticles supported on polydopamine-functionalized graphene and their high performance toward 4- nitrophenol reduction, Appl. Catal. B 181 (2016) 371–378.
[43] Y. Fu, P. Li, Q. Xie, X. Xu, L. Lei, C. Chen, C. Zou, W. Deng, S. Yao, One-pot preparation of polymer–enzyme–metallic nanoparticle composite films for high-performance biosensing of glucose and galactose, Adv. Funct. Mater. 19 (2009) 1784–1791.
[44] T. Zeng, X.-L. Zhang, H.-Y. Niu, Y.-R. Ma, W.-H. Li, Y.-Q. Cai, In situ growth of gold nanoparticles onto polydopamine-encapsulated magnetic microspheres for catalytic reduction of nitrobenzene, Appl. Catal. B 134 (2013) 26–33.
[45] N. Zhu, Y. Cao, C. Shi, P. Wu, H. Ma, Biorecovery of gold as nanoparticles and its catalytic activities for p-nitrophenol degradation, Environ. Sci. Pollut. Res. Int. 23 (2016) 7627–7638.
[46] W. Shen, Y. Qu, X. Pei, S. Li, S. You, J. Wang, Z. Zhang, J. Zhou, Catalytic reduction of 4-nitrophenol using gold nanoparticles biosynthesized by cell-free extracts of Aspergillus sp. WL-Au, J. Hazard. Mater. 321 (2017) 299–306.
[47] B. Vellaichamy, P. Periakaruppan, Catalytic hydrogenation performance of in-Situ assembled Au@g-C_3N_4-PANI nanoblend: synergistic inter-constituent interactions boost the catalysis, New J. Chem. 7123–7132 (2017).
[48] T. Sano, S. Tsutsui, K. Koike, T. Hirakawa, Y. Teramoto, N. Negishi, K. Takeuchi, Activation of graphitic carbon nitride (g-C_3N_4) by alkaline hydrothermal treatment for photocatalytic NO oxidation in gas phase, J. Mater. Chem. A 1 (2013) 6489–6496.
[49] C. Shi, N. Zhu, Y. Cao, P. Wu, Biosynthesis of gold nanoparticles assisted by the intracellular protein extract of *Pycnoporus sanguineus* and its catalysis in degradation of 4-nitroaniline, Nanoscale Res. Lett. 10 (2015) 147.
[50] T.Y. Ma, Y. Tang, S. Dai, S.Z. Qiao, Proton-functionalized two-dimensional graphitic carbon nitride nanosheet: an excellent metal-/label-free biosensing platform, Small 10 (2014) 2382–2389.
[51] X. Zhang, X. Xie, H. Wang, J. Zhang, B. Pan, Y. Xie, Enhanced photoresponsive ultrathin graphitic-phase C_3N_4 nanosheets for bioimaging, JACS 135 (2012) 18–21.
[52] W.-J. Ong, L.-L. Tan, S.-P. Chai, S.-T. Yong, A.R. Mohamed, Surface charge modification via protonation of graphitic carbon nitride (g-C_3N_4) for electrostatic self-assembly construction of 2D/2D reduced graphene oxide (rGO)/g-C_3N_4 nanostructures toward enhanced photocatalytic reduction of carbon dioxide to methane, Nano Energy 13 (2015) 757–770.
[53] Y. Fu, J. Zhu, C. Hu, X. Wu, X. Wang, Covalently coupled hybrid of graphitic carbon nitride with reduced graphene oxide as a superior performance lithium-ion battery anode, Nanoscale 6 (2014) 12555–12564.
[54] N. Cheng, J. Tian, Q. Liu, C. Ge, A.H. Qusti, A.M. Asiri, A.O. Al-Youbi, X. Sun, Au-nanoparticle-loaded graphitic carbon nitride nanosheets: green photocatalytic synthesis and application toward the degradation of organic pollutants, ACS Appl. Mater. Interfaces 5 (2013) 6815–6819.
[55] Q. Xiang, J. Yu, M. Jaroniec, Preparation and enhanced visible-light photocatalytic H2-production activity of graphene/C_3N_4 composites, J. Phys. Chem. C 115 (2011) 7355–7363.
[56] Q. Lu, J. Zhang, X. Liu, Y. Wu, R. Yuan, S. Chen, Enhanced electrochemiluminescence sensor for detecting dopamine based on gold nanoflower@ graphitic carbon nitride polymer nanosheet–polyaniline hybrids, Analyst 139 (2014) 6556–6562.
[57] V.K. Gupta, N. Atar, M.L. Yola, Z. Üstündağ, L. Uzun, A novel magnetic Fe@Au core–shell nanoparticles anchored graphene oxide recyclable nanocatalyst for the reduction of nitrophenol compounds, Water Res. 48 (2014) 210–217.
[58] S. Praharaj, S. Nath, S.K. Ghosh, S. Kundu, T. Pal, Immobilization and recovery of Au nanoparticles from anion exchange resin: resin-bound nanoparticle matrix as a catalyst for the reduction of 4-nitrophenol, Langmuir 20 (2004) 9889–9892.
[59] Y. Mei, Y. Lu, F. Polzer, M. Ballauff, M. Drechsler, Catalytic activity of palladium nanoparticles encapsulated in spherical polyelectrolyte brushes and core−shell microgels, Chem. Mater. 19 (2007) 1062–1069.
[60] N.C. Sharma, S.V. Sahi, S. Nath, J.G. Parsons, J.L. Gardea- Torresde, T. Pal, Synthesis of plant-mediated gold nanoparticles and catalytic role of biomatrix-embedded nanomaterials, Environ. Sci. Technol. 41 (2007) 5137–5142.
[61] A. Liu, C.H.H. Traulsen, J.J.L.M. Cornelissen, Nitroarene reduction by a virus protein cage based nanoreactor, ACS Catal. 6 (2016) 3084–3091.
[62] J.-J. Lv, A.-J. Wang, X. Ma, R.-Y. Xiang, J.-R. Chen, J.-J. Feng, One-pot synthesis of porous Pt-Au nanodendrites supported on reduced graphene oxide nanosheets toward catalytic reduction of 4-nitrophenol, J. Mater. Chem. A 3 (2015) 290–296.
[63] C. Chu, Z. Su, Facile synthesis of AuPt alloy nanoparticles in polyelectrolyte multilayers with enhanced catalytic activity for reduction of 4-nitrophenol, Langmuir 30 (2014) 15345–15350.
[64] M. Pan, A.J. Brush, Z.D. Pozun, H.C. Ham, W.-Y. Yu, G. Henkelman, G.S. Hwang, C.B. Mullins, Model studies of heterogeneous catalytic hydrogenation reactions with gold, Chem. Soc. Rev. 42 (2013) 5002–5013.
[65] K.-I. Shimizu, Y. Miyamoto, T. Kawasaki, T. Tanji, Y. Tai, A. Satsuma, Chemoselective hydrogenation of nitroaromatics by supported gold catalysts: mechanistic reasons of size-and support-dependent activity and selectivity, J. Phys. Chem. C 113 (2009) 17803–17810.
[66] J.A. van Bokhoven, J.T. Miller, d Electron density and reactivity of the d band as a function of particle size in supported gold catalysts, J. Phys. Chem. C 111 (2007) 9245–9249.
[67] B. Vellaichamy, P. Periakaruppan, Catalytic hydrogenation performance of an in situ assembled Au@g-C_3N_4-PANI nanoblend: synergistic inter-constituent interactions boost the catalysis, New J. Chem. 41 (2017) 7123–7132.
[68] K.B. Narayanan, N. Sakthivel, Synthesis and characterization of nano-gold composite using Cylindrocladium floridanum and its heterogeneous catalysis in the degradation of 4-nitrophenol, J. Hazard. Mater. 189 (2011) 519–525.
[69] F. Liu, X. Liu, D. Astruc, H. Gu, Dendronized triazolyl-containing ferrocenyl polymers as stabilizers of gold nanoparticles for recyclable two-phase reduction of 4-nitrophenol, J. Colloid Interface Sci. 533 (2019) 161–170.
[70] S.K. Maji, A. Jana, Two-dimensional nanohybrid (RGS@AuNPs) as an effective catalyst for the reduction of 4-nitrophenol and photo-degradation of methylene blue dye, New J. Chem. 41 (2017) 3326–3332.
[71] P. Guo, L. Tang, J. Tang, G. Zeng, B. Huang, H. Dong, Y. Zhang, Y. Zhou, Y. Deng, L. Ma, Catalytic reduction–adsorption for removal of p-nitrophenol and its conversion p-aminophenol from water by gold nanoparticles supported on oxidized mesoporous carbon, J. Colloid Interface Sci. 469 (2016) 78–85.
[72] F. Cárdenas-Lizana, Z.M. De Pedro, S. Gómez-Quero, L. Kiwi-Minsker, M.A. Keane, Carbon supported gold and silver: application in the gas phase hydrogenation of m-dinitrobenzene, J. Mol. Catal. A: Chem. 408 (2015) 138–146.
[73] X. Wang, J. Fu, M. Wang, Y. Wang, Z. Chen, J. Zhang, J. Chen, Q. Xu, Facile synthesis of Au nanoparticles supported on polyphosphazene functionalized carbon nanotubes for catalytic reduction of 4-nitrophenol, J. Mater. Sci. 49 (2014) 5056–5065.
[74] J. Xia, G. He, L. Zhang, X. Sun, X. Wang, Hydrogenation of nitrophenols catalyzed by carbon black-supported nickel nanoparticles under mild conditions, Appl. Catal. B 180 (2016) 408–415.
[75] Z. Zhang, C. Shao, Y. Sun, J. Mu, M. Zhang, P. Zhang, Z. Guo, P. Liang, C. Wang, Y. Liu, Tubular nanocomposite catalysts based on size-controlled and highly dispersed silver nanoparticles assembled on electrospun silica nanotubes for catalytic reduction of 4-nitrophenol, J. Mater. Chem. 22 (2012) 1387–1395.
[76] Y. Ge, T. Gao, C. Wang, Z.H. Shah, R. Lu, S. Zhang, Highly efficient silica coated CuNi bimetallic nanocatalyst from reverse microemulsion, J. Colloid Interface Sci. 491 (2017) 123–132.
[77] Y. Tuo, G. Liu, B. Dong, J. Zhou, A. Wang, J. Wang, R. Jin, H. Lv, Z. Dou, W. Huang, Microbial synthesis of Pd/$Fe_{(3)}O_{(4)}$, Au/$Fe_{(3)}O_{(4)}$ and PdAu/$Fe_{(3)}O_{(4)}$ nanocomposites for catalytic reduction of nitroaromatic compounds, Sci. Rep. 5 (2015) 13515.
[78] J. Sun, Y. Fu, G. He, X. Sun, X. Wang, Catalytic hydrogenation of nitrophenols and nitrotoluenes over a palladium/graphene nanocomposite, Catal. Sci. Technol. 4 (2014) 1742–1748.
[79] K. Layek, M.L. Kantam, M. Shirai, D. Nishio-Hamane, T. Sasaki, H. Maheswaran, Gold nanoparticles stabilized on nanocrystalline magnesium oxide as an active catalyst for reduction of nitroarenes in aqueous medium at room temperature, Green Chem. 14 (2012) 3164–3174.
[80] W. Ye, D. Wang, H. Zhang, F. Zhou, W. Liu, Electrochemical growth of flowerlike gold nanoparticles on polydopamine modified ITO glass for SERS application, Electrochim. Acta 55 (2010) 2004–2009.
[81] S. Wunder, F. Polzer, Y. Lu, Y. Mei, M. Ballauff, Kinetic analysis of catalytic reduction of 4-nitrophenol by metallic nanoparticles immobilized in spherical polyelectrolyte brushes, J. Phys. Chem. C 114 (2010) 8814–8820.
[82] S. Giri, R. Das, C.V.D. Westhuyzen, A. Maity, An efficient selective reduction of nitroarenes catalyzed by reusable silver-adsorbed waste nanocomposite, Appl. Catal. B 209 (2017) 669–678.
[83] H. Li, M. Yang, J. Liu, Y. Zhang, Y. Yang, H. Huang, Y. Liu, Z. Kang, A practical and highly sensitive C3N4-TYR fluorescent probe for convenient detection of dopamine, Nanoscale 7 (2015) 12068–12075.
[84] H.S. Oh, J.H. Yang, C.K. Costello, Y.M. Wang, S.R. Bare, H.H. Kung, M.C. Kung, Selective catalytic oxidation of CO: effect of chloride on supported Au catalysts, J. Catal. 210 (2002) 375–386.

[85] Z. Yu, F. Li, Q. Yang, H. Shi, Q. Chen, M. Xu, Nature-mimic method to fabricate polydopamine/graphitic carbon nitride for enhancing photocatalytic degradation performance, ACS Sustain. Chem. Eng. 5 (2017) 7840–7850.
[86] R. Huo, X.-L. Yang, J.-Y. Yang, S.-Y. Yang, Y.-H. Xu, Self-assembly synthesis of $BiVO_4$/Polydopamine/g-C_3N_4 with enhanced visible light photocatalytic performance, Mater. Res. Bull. 98 (2018) 225–230.
[87] H. Tada, T. Mitsui, T. Kiyonaga, T. Akita, K. Tanaka, All-solid-state Z-scheme in CdS–Au–TiO_2 three-component nanojunction system, Nat. Mater. 5 (2006) 782.
[88] L. Qu, N. Wang, H. Xu, W. Wang, Y. Liu, L. Kuo, T. Yadav, J. Wu, J. Joyner, Y. Song, Gold nanoparticles and g-C_3N_4-intercalated graphene oxide membrane for recyclable surface enhanced Raman scattering, Adv. Funct. Mater. 27 (2017) 1701714.